Regular Article

PHYSICAL CHEMISTRY RESEARCH
Published by the
Iranian Chemical Society
www.physchemres.org
info@physchemres.org

***Phys. Chem. Res.**, Vol. 8, No. 1, 1-18, March 2020*
DOI: 10.22036/pcr.2019.205211.1688

Biosynthesis of Silver Nanoparticles Using Leaves of Acacia Melanoxylon and their Application as Dopamine and Hydrogen Peroxide Sensors

R. Shashanka[a,*] and B.E. Kumara Swamy[b]

[a]*Department of Metallurgical and Materials Engineering, Bartin University, Bartin-74100, Turkey*
[b]*Department of P.G. Studies and Research in Industrial Chemistry, Kuvempu University, Jnana Sahyadri, Shankaraghatta 577451, Shimoga, Karnataka, India*

(Received 14 October 2019, Accepted 2 November 2019)

In this work, we described a cost-effective and environmentally friendly technique for green synthesis of colloidal silver nanoparticles from an aqueous extract of fresh leaves of Acacia melanoxylon and their application as a dopamine and hydrogen peroxide sensor. The prepared silver nanoparticles were characterized using UV-Vis absorption spectroscopy, X-ray diffraction (XRD), scanning electron microscopy (SEM), zeta-potential analysis, thermogravimetric analysis (TGA), differential scanning calorimeter (DSC), *etc*. This method was found to be cost-effective, eco-friendly when compared to that of chemical and physical methods of nanoparticle synthesis. Silver nanoparticles modified carbon paste electrode (CPE) was fabricated for the detection of dopamine and hydrogen peroxide. The fabricated electrode showed an excellent sensitivity towards the oxidation of both dopamine (DA) and hydrogen peroxide (H_2O_2) in 0.1 M phosphate buffer (PBS) solution at pH 7. The effects of scan rate, and concentration of the modifier and analyte were studied by the cyclic voltammetric technique. The result exhibits good electrocatalytic activity, diffusion-controlled process and linear increase in peak current with different concentrations of dopamine and hydrogen peroxide.

Keywords: Silver nanoparticles, Cyclic voltammetry, Acacia melanoxylon, Dopamine, Hydrogen peroxide

INTRODUCTION

Different methods are available for the synthesis of different sized nanoparticles among which the biological-based techniques are more popular and widely used. The use of biological organisms such as microorganisms, and plant extract could be an alternative to chemical and physical methods for the production of nanoparticles [1]. In recent years, plant-mediated biological synthesis of nanoparticles is gaining importance due to its simplicity and eco-friendliness. The research articles regarding biosynthesis of gold and silver nanoparticles by plants such as Alfalfa, Aloe vera, Cinnamomum camphora, Emblica officianalis, Carica papaya, Parthenium hysterophorus, Diopyros kaki, Azadirachta indica, Eucalyptus hybrid, Hibiscus rosasinensis, and Capsicum annuum have been reported elsewhere [2-6]. Acacia melanoxylon is another type of plant used to prepare silver nanoparticles. Acacia melanoxylon is a common tree usually found in the southern part of India. The timber wood of Acacia melanoxylon is very good for many uses including furniture, tools, boats, and wooden kegs. It is of the same quality as walnut and it is well-suited for shaping with steam and can also be used for producing decorative veneers. The tree's twigs and its bark are used to poison fish as a way of fishing [7].

It has been reported that extra-cellularly prepared silver nanoparticles can be dispersed in various kinds of materials such as cloths; these silver cloths are highly sterile and hence find their application in hospitals. These cloths are used to prevent or to minimize the infection with pathogenic bacteria. Biosynthesized silver nanoparticles are unique compared to the silver nanoparticles prepared from

*Corresponding author. E-mail: shashankaic@gmail.com

chemical or physical methods and hence used in wide range of applications such as bio-labelling, in nonlinear optics, spectrally selective coating for solar energy absorption, intercalation materials for electrical batteries, as optical receptors, catalyst in chemical reactions and as an antibacterial material [8].

Dopamine and hydrogen peroxide are the common and very important intermediates in both environmental and biological systems, whose reliability, rapid and economic determination remains an important topic pertaining to environmental, pharmaceutical, clinical and industrial research [9]. Dopamine is one of the most important neurotransmitters present in the mammalian central nervous system. It is a catecholamine in the form of large organic cations and belongs to the family of excitatory chemical neurotransmitters [10]. It plays an important role in the functioning of the central nervous, renal, cardiovascular and hormonal systems as well as in Parkinson's disease [11]. Even hydrogen peroxide seems to have a toxic effect in patients with Parkinson's disease [12]. Changes in DA concentration in biological samples are an important indication of possible body abnormalities or diseases. On the other hand H_2O_2, due to its direct oxidation at the bare electrode, slow electrode kinetics and high overpotential required for redox reactions made it not suitable for analytical applications. Some of the electrochemical methods have been proved to be an effective and inexpensive way for both DA and H_2O_2 determination. Therefore, the determination of DA and H_2O_2 has become important and been given tremendous attention by neuroscientists and chemists in biomedical and bioanalytical research. Some of the bioactive materials possess the high electrochemical activity and hence there will be large lacunae to study electroanalytical techniques significantly to benefit biosciences. So, it is important to establish a fast, sensitive method for the detection of both DA and H_2O_2 by the modification of bare electrodes making their detection possible by electrochemical methods based on anodic oxidation [13]. During the last decades, new electrodes using organic molecules as a modifier have been developed and widely used due to their ease of construction and low cost. The modification of these electrodes is very simple because it requires only mixing the modifier with the carbon paste in a mortar. In this way, it is possible to add a wide variety of products such as inorganic or organic substances, biomolecules, animal or plant tissues, etc. as modifiers [14]. Hence, the preparation of the modified carbon paste electrode (MCPE) with catalytic function is of practical significance.

In the present paper, we successfully fabricated the silver nanoparticles modified carbon paste electrode and studied their electrochemical properties in detail by using cyclic voltammetry. We proved that silver nanoparticles are a kind of suitable mediators to determine the DA even in low concentrations. Generally, a high overpotential is required for the red-ox reaction of H_2O_2, however in the present paper, we showed that the fabricated silver nanoparticle modified carbon paste electrode reduces the electrochemical oxidation/reduction overpotential of H_2O_2. The silver nanoparticles modified electrode showed good electrocatalytic oxidation of both dopamine and H_2O_2. On the basis of the electrochemical response of dopamine and H_2O_2, the silver nanoparticle modified carbon paste electrode can be used for the development of the sensor.

EXPERIMENTAL

Reagents and Chemicals

AR grade silver nitrate was purchased from Himedia chemical company. Dopamine, perchloric acid, Hydrogen peroxide, sodium dihydrogen orthophosphate dehydrate and di-sodium hydrogen phosphate anhydrous used were of analytical grade quality from S.D. Fine chemicals. All the above reagents solutions were prepared by dissolving in double-distilled water. Graphite powder was purchased from Merck chemicals.

Apparatus

The electrochemical experiments were carried out using the electrochemical work station CHI-660c model. All the experiments were carried out in a conventional three-electrode electrochemical cell. The electrode system was composed of a 3mm carbon paste electrode as a working electrode, a platinum wire as a counter electrode and Ag/AgCl saturated KCl electrode as a reference electrode. Scanning electron microscopy (SEM) image was obtained using a JEOL. X-ray diffraction studies were performed using PAN analytical Xpert Pro XRD. Zeta potential was

performed using in Zeta trac-microtrac (Malvern, USA). The pH of the buffer solution was measured with the digital pH meter MK VI. IR spectra were collected in Jasco FTIR 460 plus. Thermogravimetric analysis was carried out using NETZSCH (Germany).

Fabrication of the Carbon Paste Electrode

The carbon paste electrode (CPE) was prepared by hand-mixing of graphite powder and silicon oil at a ratio of 70:30 in an agitate mortar [15,16]. The homogeneous carbon paste electrode was packed into a cavity of a homemade carbon paste electrode (3.0 mm in diameter). The prepared nanoparticles were in a colloidal solution; hence modifier was taken in µl. The Ag nanoparticle modified carbon paste electrode (SNCPE) was prepared by mixing a colloidal solution of Ag nanoparticles with graphite powder and silicon oil. Surface was smoothened on a piece of weighing paper [17]. The electrical contact was provided by a copper wire connected to the paste at the end of the tube. The bare CPE was prepared without adding a modifier (silver nanoparticles).

Synthesis of Silver Nanoparticles Using Acacia Melanoxylon Broth

Acacia melanoxylon plant leaves were collected from Kuvempu University, India with the help of an expert. Ten grams of freshly collected healthy leaves of Acacia melanoxylon were taken and washed thoroughly in flush of tap water in the laboratory for 10 min in order to remove the dust particles and then cut into small pieces and rinsed briefly in sterile distilled water. Then, the sample was placed in a 250 ml beaker containing 100 ml distilled water and was placed on a boiling steam bath for 15 to 20 min until the color of the solvent changes to light yellow. Figures 1a and 1b represent the acacia melanoxylon leaves and the plant extract before and after the formation of silver nanoparticles. Shashanka *et al.* [18] reported the detailed procedure of the synthesis of silver nanoparticles by Acacia melanoxylon leaves.

The extract was filtered through sterile filter paper and this solution was treated as source extract. Then, 5 ml extract solution was treated with 50 ml of 0.01 M $AgNO_3$ solution and warmed again on the steam bath for 10 min until the color of the solution changes to reddish-brown and was allowed to cool and incubate in the laboratory ambiance. Concurrently, ultraviolet-visible (UV-Vis) spectrophotometric study was performed at different time intervals. The plant extract can be stored at a very low temperature to avoid fungal growth and the same can be used for further research work.

RESULTS AND DISCUSSION

UV-Vis Analysis of Silver Nanoparticles

UV-Vis spectroscopy is an important technique used to investigate the formation and stability of metal nanoparticles in aqueous solution. The color of silver nanoparticle colloidal solution is attributed to surface plasmon resonance (SPR) arising due to the collective oscillation of free conduction electrons induced by an interacting electromagnetic field. Figures 2a and 2b show the UV-Vis spectra of the colloidal silver nanoparticles obtained after 15 min of reaction and with different time intervals, respectively. The absorption peak at 435 nm confirms the formation of silver nanoparticles and is probably related to the electronic transition taking place from the valence band to the conduction band.

X-Ray Diffraction Study

The nanocrystalline nature and the phases of Ag nanoparticles prepared from the above method were confirmed from the X-ray diffraction analysis. Figure 3 shows the XRD pattern of Ag nanoparticles prepared from acacia melanoxylon leaf extract. The diffraction peaks obtained at 38.10°, 44.27° and 64.42° correspond to the (111), (200) and (220) planes of the face-centered cubic crystal structure respectively. The (111) peak is more dominant than the other peaks. Hence, the average crystallite size of the prepared silver nanoparticle was calculated from the width of (111) peak using the Scherrer equation and it is found to be ~10 nm. The experimental diffraction angles and Standard diffraction angles are enumerated in Table 1. The intensities and positions of peaks are in a good agreement with the reported values in JCPDS file no. 04-0783.

Calculation of radius and the intensity ratio of diffraction peaks. The FCC crystal structure of the prepared silver nanoparticles has a unit cell edge

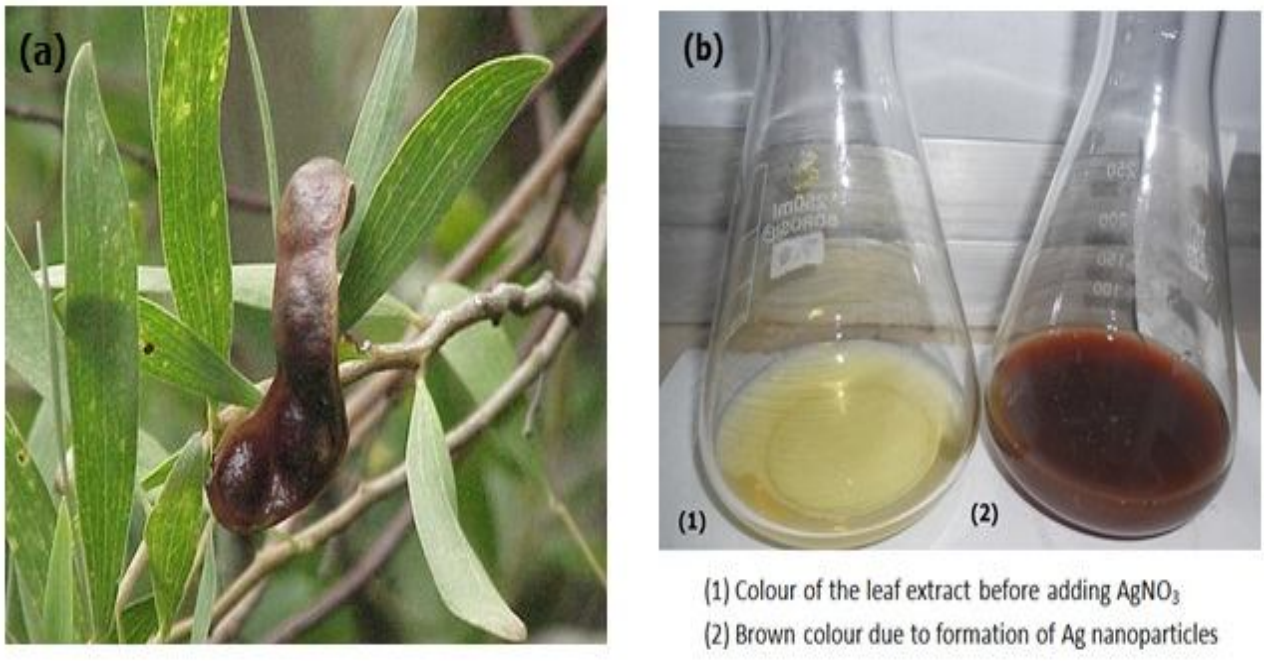

Fig. 1. (a) Acacia melanoxylon leaves. (b) Color change of the leaf extract before and after synthesis of Ag nanoparticles.

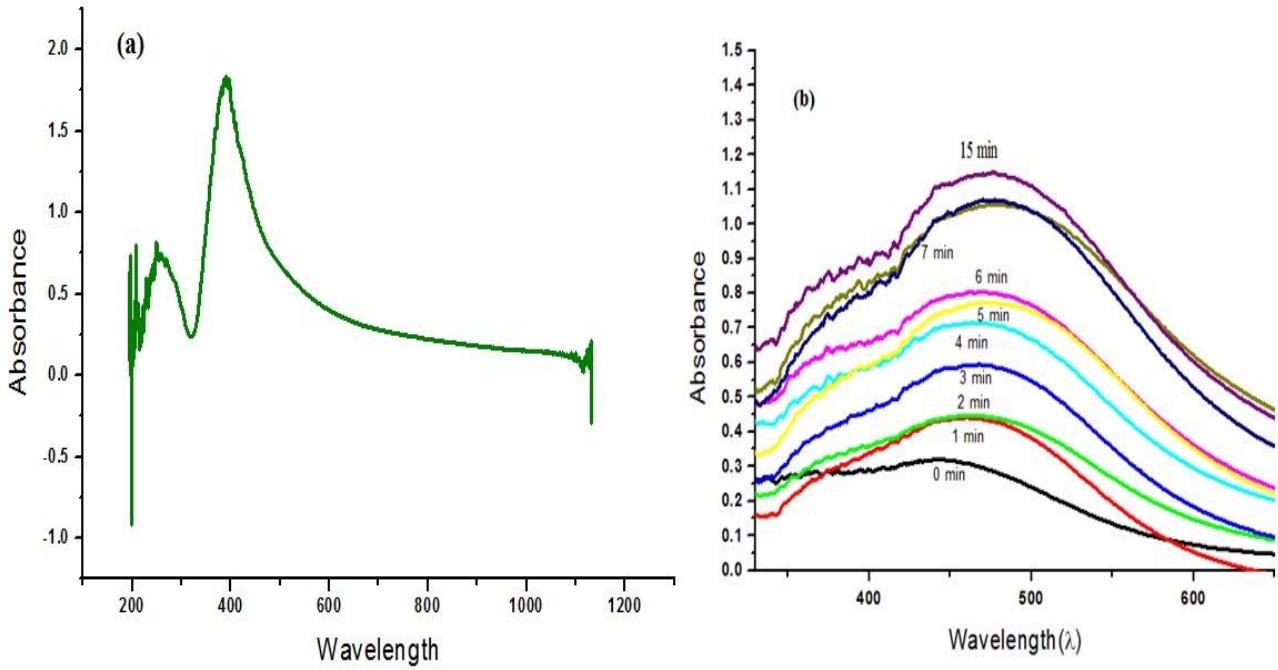

Fig. 2. (a) The UV-Vis spectra of the silver colloids obtained after 15 min of reaction, and (b) the UV-Vis spectra with different time intervals from 0 to 15 min.

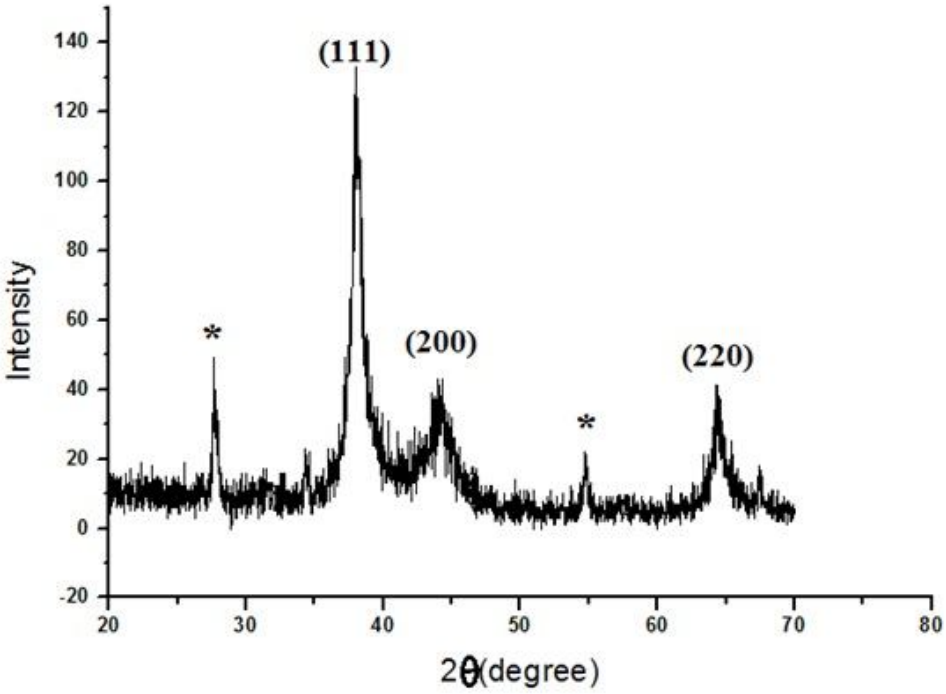

Fig. 3. XRD of as-prepared Ag nanoparticles.

Table 1. Ratio between the Intensities of the Diffraction Peaks

Diffraction peaks	Sample value	Conventional value
(200) and (111)	0.3255	0.40
(220) and (111)	0.3087	0.25

'*a*' = 4.086 Å. The value of the silver radius (r) can be calculated from Eq. (1) and 'r' value of the prepared silver nanoparticle was found to be 1.44 Å.

$$r = \frac{a}{2\sqrt{2}} \tag{1}$$

The theoretically calculated value of 'a' from Eq. (1) is 4.086 Å. Both theoretical and experimental values of lattice constant 'a' are in agreement with the JCPDS file no. 04-0783. The ratio between the intensities of the (200) and (111) diffraction peaks and (220) and (111) diffraction peaks were tabulated in Table 1. The ratio between the intensities of the (200) and (111) diffraction peaks is slightly lower than the conventional value (0.3255 versus 0.40), but that of (220) and (111) peaks is slightly greater than the conventional value (0.3087 *versus* 0.25) which is due to the relative abundance of {100} facets in our prepared silver nanoparticles.

XRD-Crystallite size calculation. Considering the diffraction peaks at Bragg's diffraction angle, the average grain size has been calculated using the Debye-Scherrer formula [19].

$$D = \frac{0.94\lambda}{\beta \cos\theta} \tag{2}$$

Where 'λ' is the wavelength of X-Ray (1.54 Å, for Cu target), 'β' is full-width half maxima (FWHM) value, 'θ' is the diffraction angle and 'D' is the grain or crystallite size. The lattice constant '*a*', peak index and the value of d-spacing particulars have been tabulated in Table 2. The average grain size of prepared silver nanoparticles is ~10 nm. The value of d (interplanar distance between the atoms) is calculated using Bragg's law as shown in Eq. (3).

$$n\lambda = 2d\sin\theta \tag{3}$$

XRD-Instrumental broadening. The crystallite size and lattice strain are calculated using the Williamson-Hall equation [20-23]. This equation is used to calculate peak broadening of the diffraction pattern due to instrumental errors.

$$\beta\cos\theta = \frac{0.94\lambda}{D} + 4\varepsilon\sin\theta \tag{4}$$

Where 'β' is FWHM, 'ε' is the lattice strain, 'D' is the average crystallite size and 'θ' is the Bragg's diffraction angle. Considerable broadening of diffraction peaks will occur mainly due to instrumental errors, a decrease in particle size, strain, *etc.* [24]. Especially, when the particle size approaches to nano level peak broadening will take place. So, the broadening errors can be minimized by using the Williamson-Hall equation. Williamson and Hall proposed a method for de-convoluting size and strain broadening by looking at the peak width as a function of 2θ. Here, Williamson-Hall plot is plotted with sin θ on the x-axis and βcosθ on the y-axis (β in radians). From the linear fit, particle size and strain are extracted from y-intercept and slope, respectively. The extracted particle size of the prepared silver nanoparticles is ~10 nm and its lattice strain is 0.0101. Figure 4 shows the Williamson-Hall plot for the green synthesized Ag nanoparticles.

XRD- Elimination of systemic errors. In the case of lattice parameters, systematic errors approach zero as θ approaches 90º and it can be eliminated by the use of a proper extrapolation function [25,26]. The slope of the extrapolation line is proportional to the magnitudes of these errors. These errors can be minimized by using the Nelson-Riley function of extrapolation. A graph of calculated lattice parameter 'a' along y-axis against $\cos^2\theta/\sin\theta + \cos^2\theta/\theta$ along x-axis is plotted. Then, the linear fit line to a value of θ = 90° is extrapolated to incur the true value of lattice constant. The calculated true lattice strain 'a' for the prepared Ag nanoparticles is 4.086 Å, as shown in Fig. 5, and the obtained values are in a very agreement with the JCPDS file no. 04-0783.

XRD- Specific surface area. Specific surface area (SSA) is a material property and an inferred scientific value that can be used to determine the type and properties of a material. In the case of nanomaterials, SSA plays an important role, as particle size decreases SSA increases. It has particular importance in case of adsorption, heterogeneous catalysis and reactions on surfaces. Generally, particle size is inversely proportional to SSA, hence it is a very essential parameter while we are dealing with nanomaterials. SSA can be calculated using Eq. (5) shown below,

$$S = \frac{6\times10^3}{D_p\times\rho} \tag{5}$$

where S is the specific surface area, D_p is the size of the nanoparticles, and ρ is the density of silver 10.5 g cm^{-3} [27]. The calculated value of SSA of the prepared silver nanoparticles is 58 m^2 g^{-1}.

XRD-Unit cell parameters. The unit cell parameters calculated from XRD are enumerated in Table 3.

Scanning Electron Microscope and EDX Analysis

In order to study the morphology of silver nanoparticles, different parts of the silver nanoparticles were focused by SEM. A typical image of green synthesized silver nanoparticles is shown in Fig. 6. It can be seen that silver nanoparticles are different shaped, and may exhibit some strange properties compared to bulk silver metal. The properties such as large specific surface area, high surface reaction and efficient transmission channel for analyte molecules to reach the active sites will help to improve the stability and sensitivity of silver nanoparticles and hence Ag nanoparticles show excellent current sensitivity for DA and H_2O_2.

A standard EDX spectrum of prepared Ag nanoparticles is shown in Fig. 7. The peaks obtained are directly related to the silver nanoparticle characteristic lines K and L. The

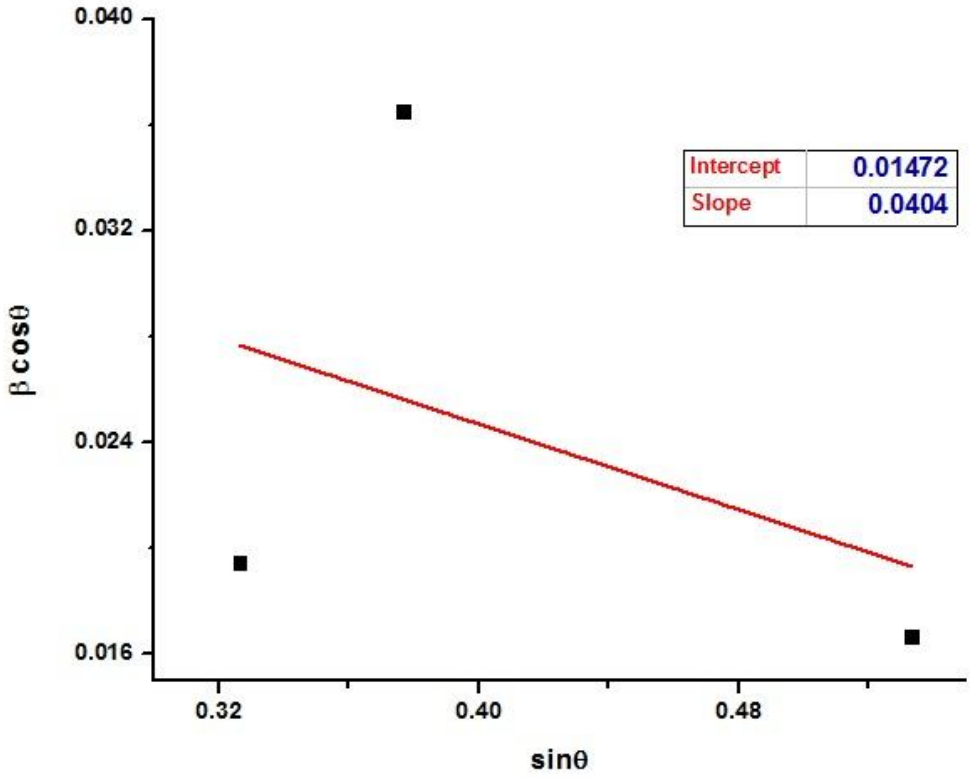

Fig. 4. Williamson-Hall plot indicating the diffraction peak broadening value due to instrumental errors.

Table 2. The d-Spacing and Lattice Parameter (a) of the Prepared Silver Nanoparticles

2θ	θ	hkl	d-spacing (Å)	Lattice parameter (Å)
38.10	19.05	(111)	2.3591	4.0861
44.27	22.135	(200)	2.0435	4.0871
64.42	32.21	(220)	1.4445	4.0859

peaks found at 0.2 keV and 0.3 keV are due to the presence of carbon and oxygen, respectively. The presence of carbon and oxygen spots in the examined samples corroborates the probability of stabilizers composed of alkyl chains [28]. The EDX analysis was performed for quantification of the prepared Ag nanoparticles and the values are found to be 69.19% for Ag, 12.04% for carbon and 18.77% for oxygen, respectively.

Zeta-potential Analysis and Particle Size Analysis

The prepared silver nanoparticles were dispersed uniformly in double-distilled water in order to study the zeta-potential. Zeta-potential is the electrical potential developed at the solid-liquid interface in response to the relative movement of the nanoparticle and the solvent. It is very important to study the electrical potential and the surface charge of the nanoparticles, because these determine

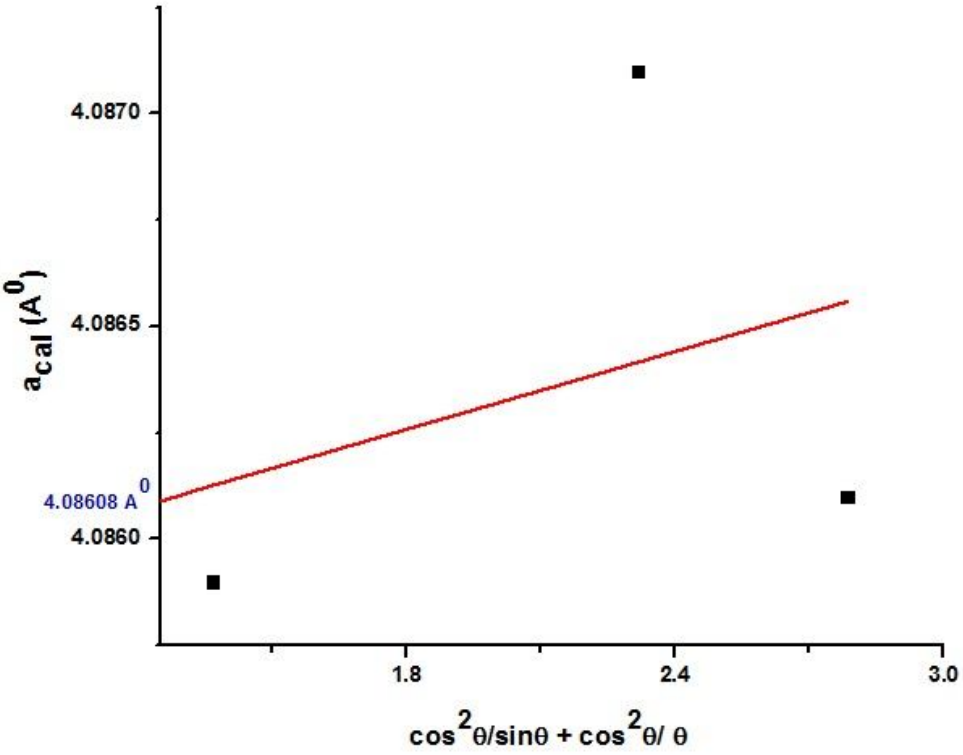

Fig. 5. Nelson-Riley function of extrapolation to determine true lattice constant 'a_o'.

Table 3. XRD Parameters of silver Nanoparticles

Parameters	Values
Structure	FCC
Space group	Fm-3m (Space group number: 225)
Point group	m3m
Packing fraction	0.74
Symmetry of lattice	cubic close-packed
Particle size	10 nm
Bond Angle	$\alpha = \beta = \gamma = 90°$
Lattice parameters	$a = b = c = 4.0860$ Å
Radius of Atom	144 pm
Density (ρ)	10.5 g cm^{-3}
Specific surface area	58 m^2 g^{-1}

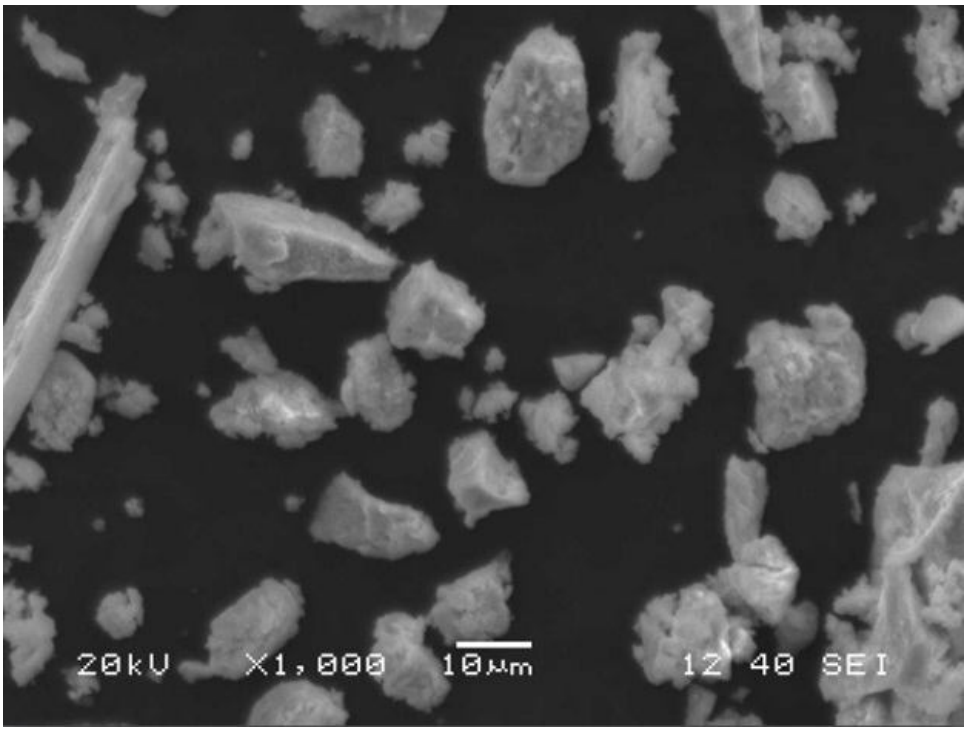

Fig. 6. SEM image of the prepared Ag nanoparticles.

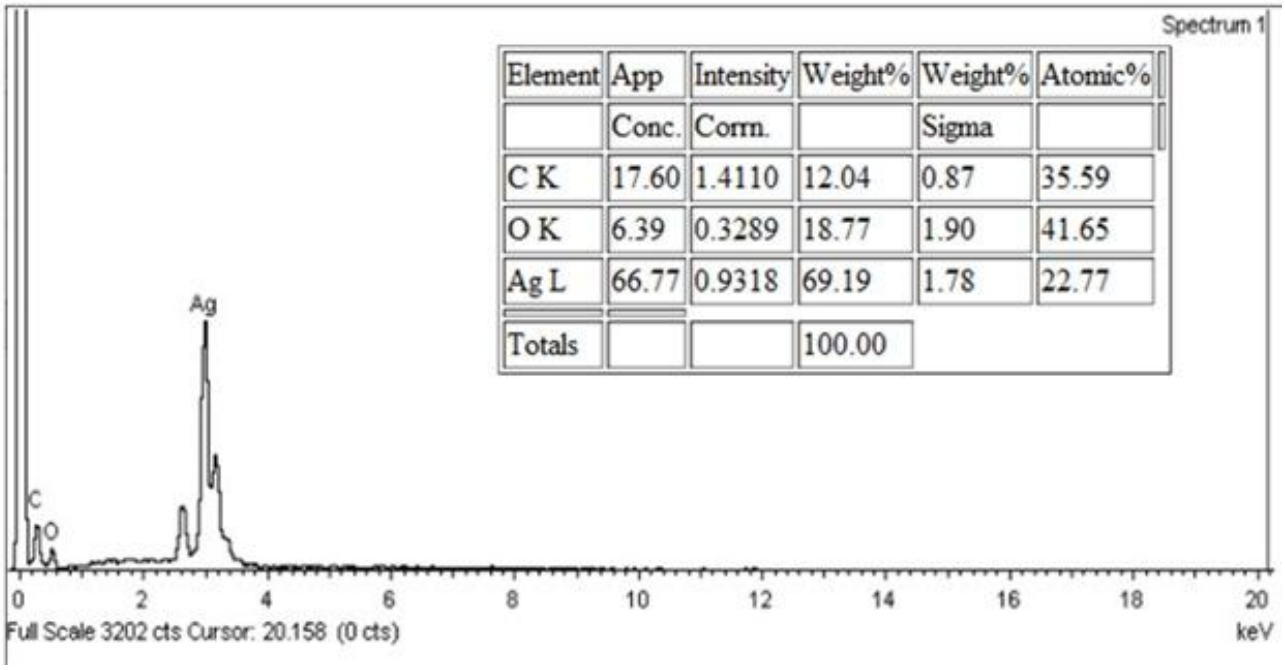

Fig. 7. EDX characteristic spectrum obtained for silver nanoparticles.

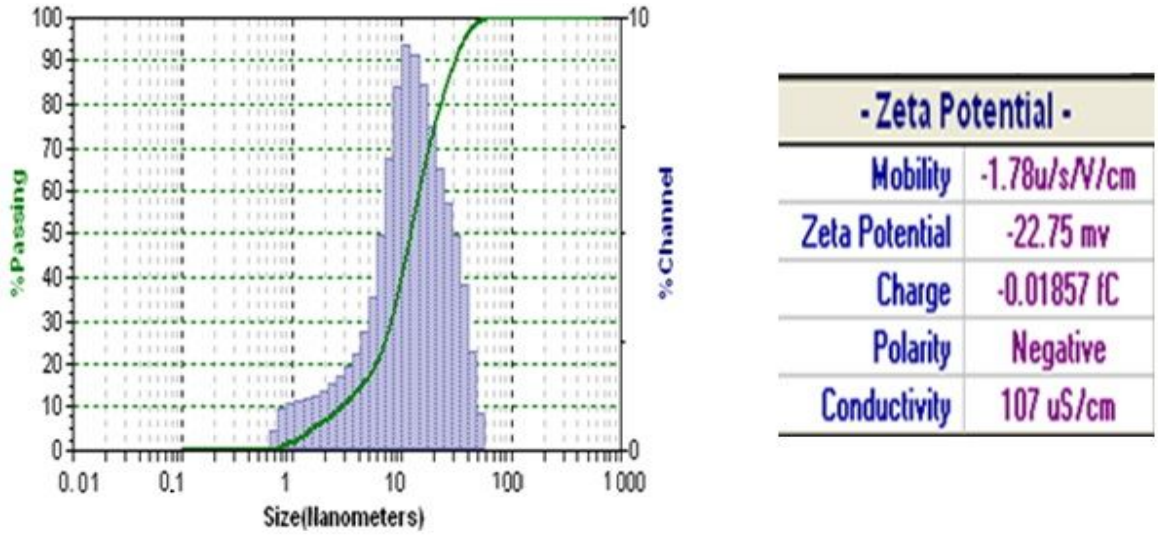

Fig. 8. Zeta potential of the as-prepared Ag nanoparticles.

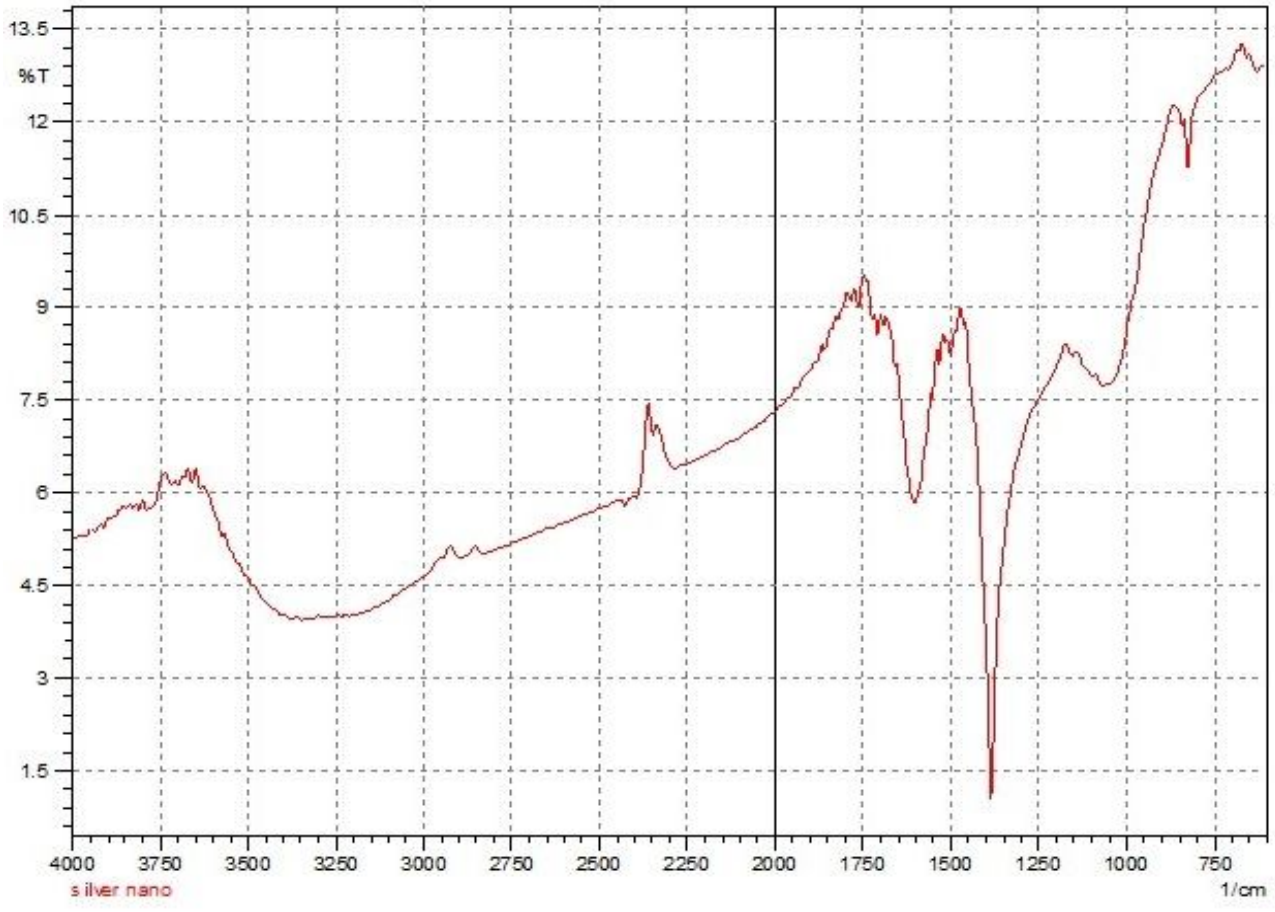

Fig. 9. FTIR spectra of Ag nanoparticles.

the stability of nanoparticles. The zeta potential of the prepared silver nanoparticles was found to be -22.75 mV. An increase in the zeta potential of the particles will increase the surface potential of charged particles. The detailed output of the zeta-potential and the particle size distribution is shown in Fig. 8. According to Zeta-potential analysis and particle size analysis, the prepared silver nanoparticles possess an average crystallite size of 10 nm which is in a good agreement with crystallite size calculated using XRD.

FTIR Spectroscopy Analysis

The prepared plant-mediated silver nanoparticles were subjected to infrared rays to identify the possible interactions between silver and bioactive compounds to determine the molecules responsible for the synthesis and stabilization (capping material) of silver nanoparticles. The amino acid residues in proteins of the plant extract give rise to amide linkages, which are well-known signatures in the infrared region of the electromagnetic spectrum. FTIR spectrum reveals two bands at 1618 and 1383 cm^{-1} corresponding to the bending vibrations of the amide I and amide II bands of the proteins, respectively. Figure 9 depicts the FTIR spectrum of the prepared silver nanoparticles. Absorbance bands observed in the region of 500-2000 cm^{-1} are 1618, 1383, 1074, 831 cm^{-1}, *etc.* These absorbance bands are known to be associated with the stretching vibrations for aromatic, C-O (esters, ethers) and C-O (polyols), respectively. In particular, the 1383cm^{-1} band arises due to the C-O group of polyols such as hydroxyflavones and catechins [29].

Thermal Analysis

Thermal analysis is very essential to investigate the sintering behavior, percentage weight loss, melting point, crystallization temperature, and glass transition temperature of the nanoparticles [30]. The thermal properties of the prepared silver nanoparticles were investigated using thermogravimetric analysis (TGA) and differential scanning calorimeter (DSC) as shown in Fig. 10. The prepared silver nanoparticle shows initial weight loss around 200 °C. The total weight loss of 23.24% is observed mainly over the temperature range from 25-800 °C with a two-step process for the samples. The first step of weight loss is in the temperature range from 150-200 °C due to the loss of moisture. Similarly, the second step involves only a small weight loss at around 450 °C that corresponds to the decomposition of oleic acid. The prepared silver nanoparticles show a sharp exothermic peak around 169 °C and a glass transition temperature (Tg) peak at 427 °C.

Electro-catalytic Response of Dopamine and H_2O_2 at Different Concentrations of Silver Nanoparticles in Carbon Paste Electrode

Both DA and H_2O_2 are easily oxidizable species that can be easily perceptible by electrochemical method showing a reversible voltammogram with a phosphate buffer solution of pH 7 as a supporting electrolyte. Figure 11 depicts the cyclic voltammogram obtained for 1×10^{-4} M of DA at BCPE (dashed line) with an anodic peak potential (Epa) at 213 mV and cathodic peak potential (Epc) at 151 mV (*vs.* SCE), respectively, in phosphate buffer solution at pH 7. The separation of redox potential peaks (ΔEp) is found to be 62 mV. However, for the silver nanoparticle modified carbon paste electrode, a pair of redox peaks is obtained with a strong increase in anodic peak current. The anodic peak potential at 221 mV and cathodic peak potential at 161 mV were obtained as shown in Fig. 11. The separation of redox potential peaks (ΔEp) was found to be 60 mV which is a characteristic of reversible voltammogram.

Similarly, Fig. 12 depicts the voltammogram of electrochemical behavior of H_2O_2 molecule in the presence of phosphate buffer solution (PBS) at pH 7 over a concentration range of 8-28 μM. The presence of silver nanoparticles in the carbon paste electrode exhibited the significant improvement of the current signal for DA and H_2O_2 and hence increases the redox peak current of DA and anodic peak current of H_2O_2 respectively.

The current sensitivity for different concentrations of silver nanoparticles has been ascertained successfully, and the anodic peak currents were compared after the addition of 10, 20, 30, 40 and 50 μl of Ag nanoparticles. Both DA and H_2O_2 showed maximum enhancement of peak current at 40 μl of silver nanoparticles as shown in Figs. 11a and 12a, respectively. The plot of anodic peak current against 10 to 50 μl concentrations of Ag nanoparticles of DA and H_2O_2 are shown in Figs. 11b and 12c, respectively. The cyclic voltammogram of H_2O_2 over the concentrations of 10 to

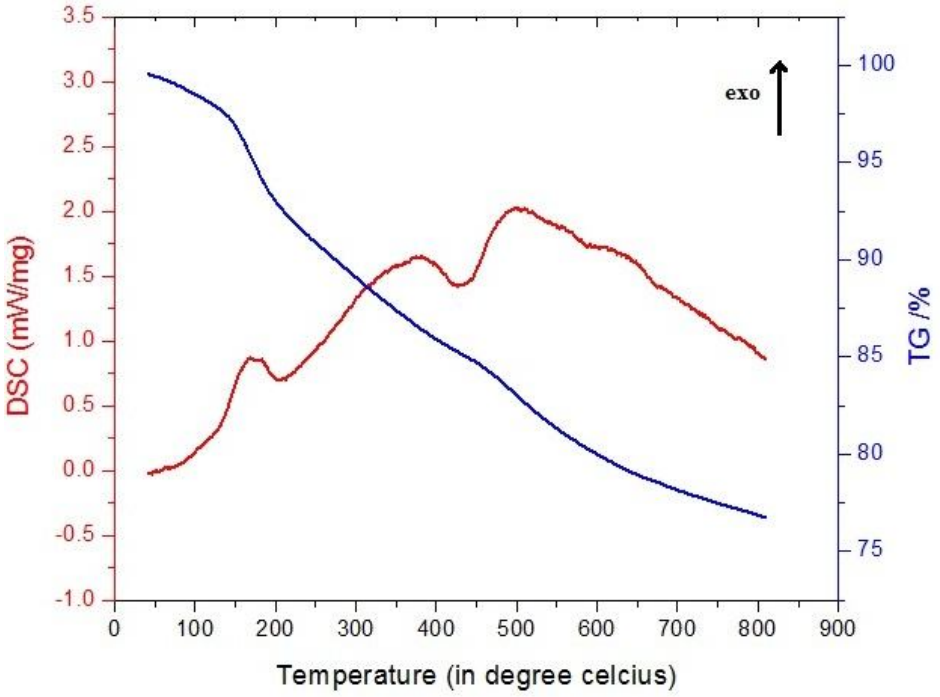

Fig. 10. TGA and DSC curves of Ag nanoparticles.

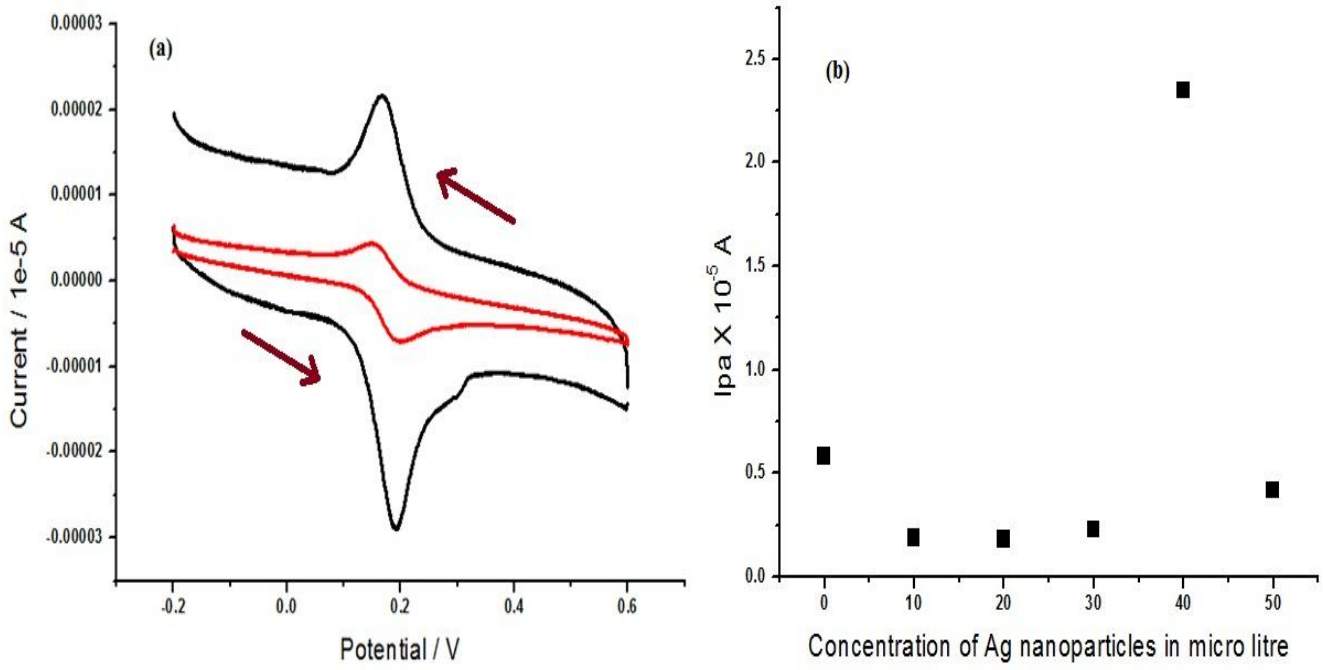

Fig. 11. (a) Cyclic voltammogram of BCPE and Ag nanoparticle MCPE for dopamine. (b) Plot of concentration variation of silver nanoparticles from 10 to 50 µl *vs*. anodic peak current at 0.1 V s^{-1} to determine dopamine.

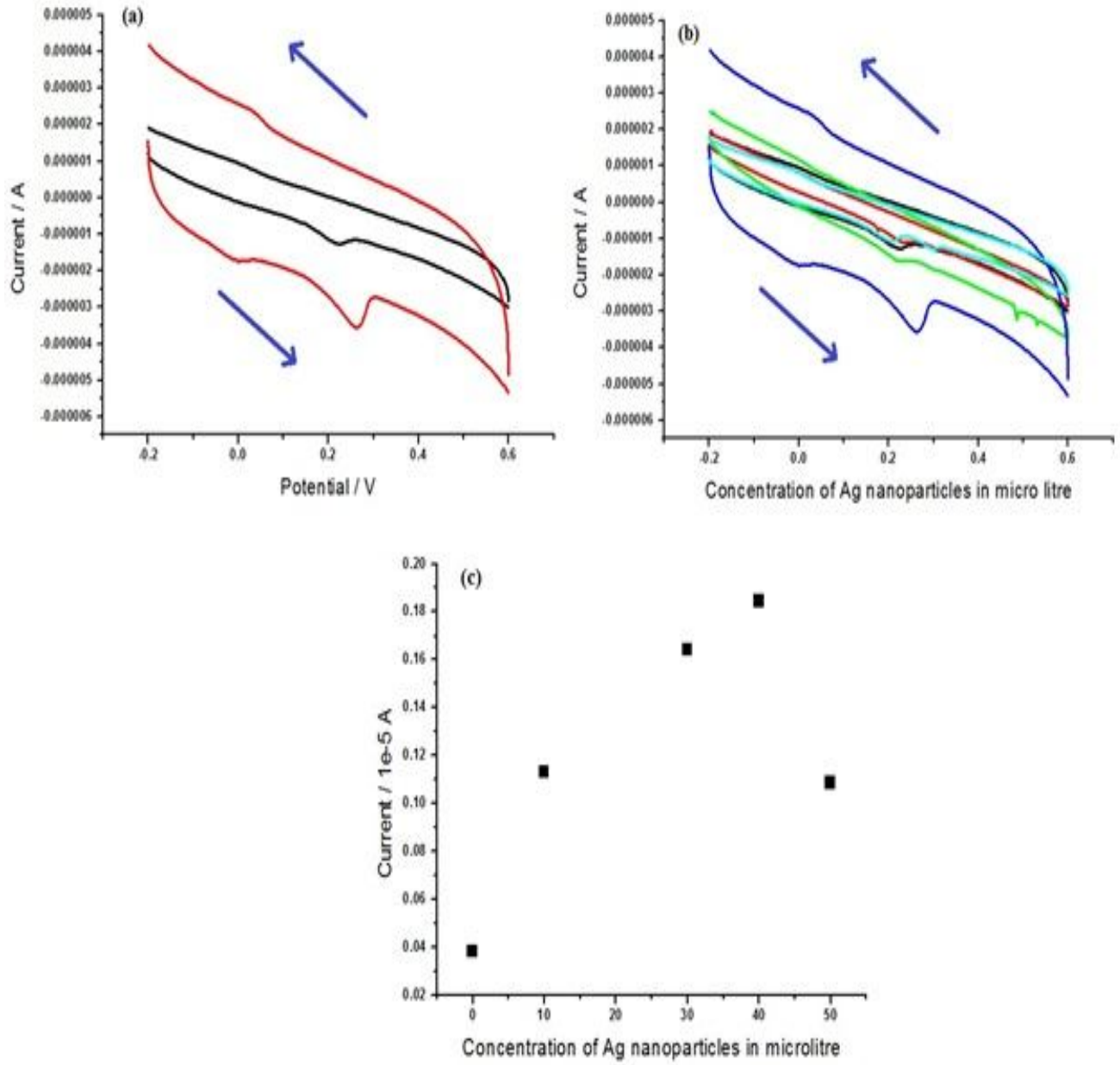

Fig. 12. (a) Cyclic voltammogram of BCPE and Ag nanoparticle MCPE for H_2O_2. (b) Cyclic voltammograms obtained for different concentrations of silver nanoparticles (10 µl to 50 µl) in PBS of pH 7 at the scan rate 100 mV s^{-1} H_2O_2 as analyte. (c) Plot of the concentration variation of silver nanoparticles from 10 to 50 µl *vs*. anodic peak current at 0.1 V s^{-1} while determining H_2O_2.

50 µl of Ag nanoparticles is as shown in Fig. 12b.

Effect of scan rate. Scan rate effect was performed by increasing the scan rate from 0.1 to 0.6 V s for 25 mM DA and from 0.1 to 0.8 V s^{-1} for 20 µM H_2O_2 in PBS of pH 7. The graphs of anodic peak current (Ipa) *vs*. square root of scan rate of DA and H_2O_2 were plotted in Figs. 13 and 14b, respectively. The MCPE shows an increase in the peak current with an increase in the scan rate. Figure 14a depicts

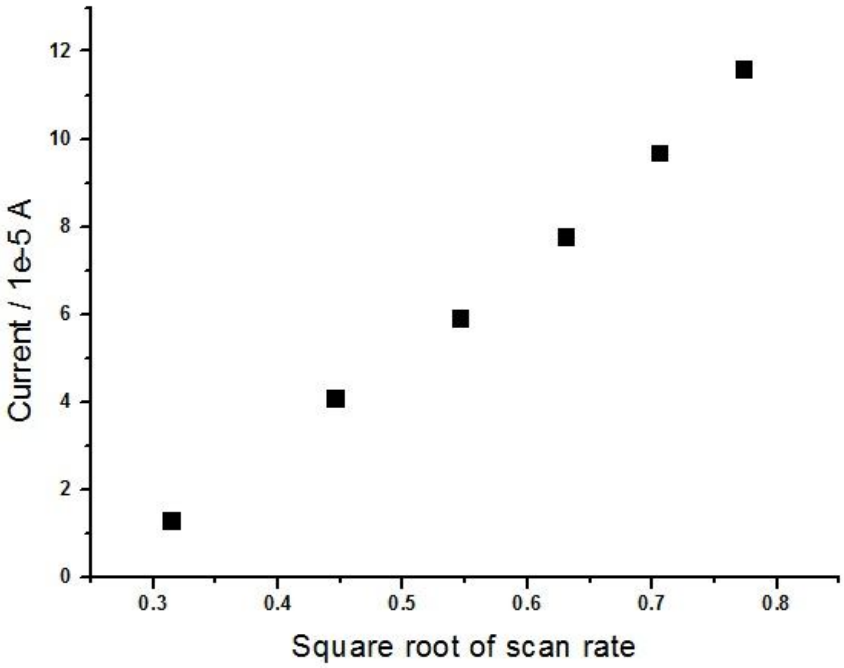

Fig. 13. Graph of peak current *vs*. square root of scan rate of dopamine.

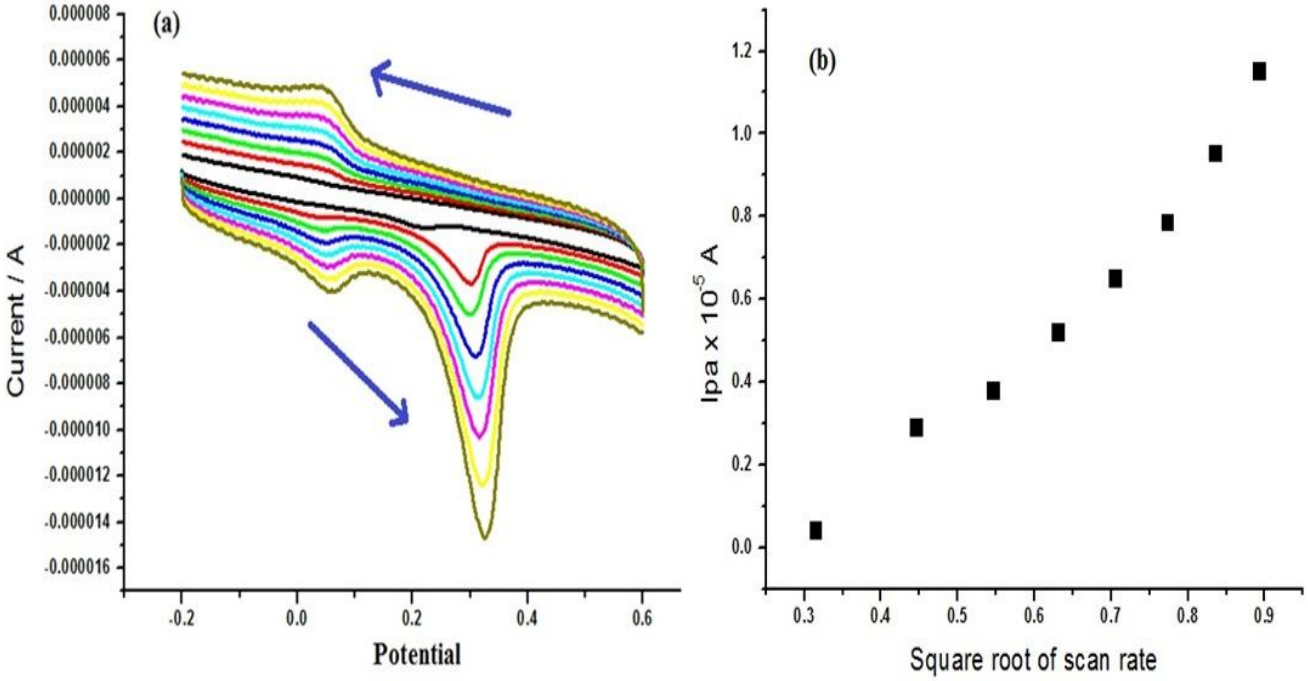

Fig. 14. (a) Cyclic voltammograms obtained for H_2O_2 at different scan rates (0.1 to 0.8 V s^{-1}) in PBS of pH 7. (b) Plot of square root of scan rate *vs*. anodic peak current for H_2O_2.

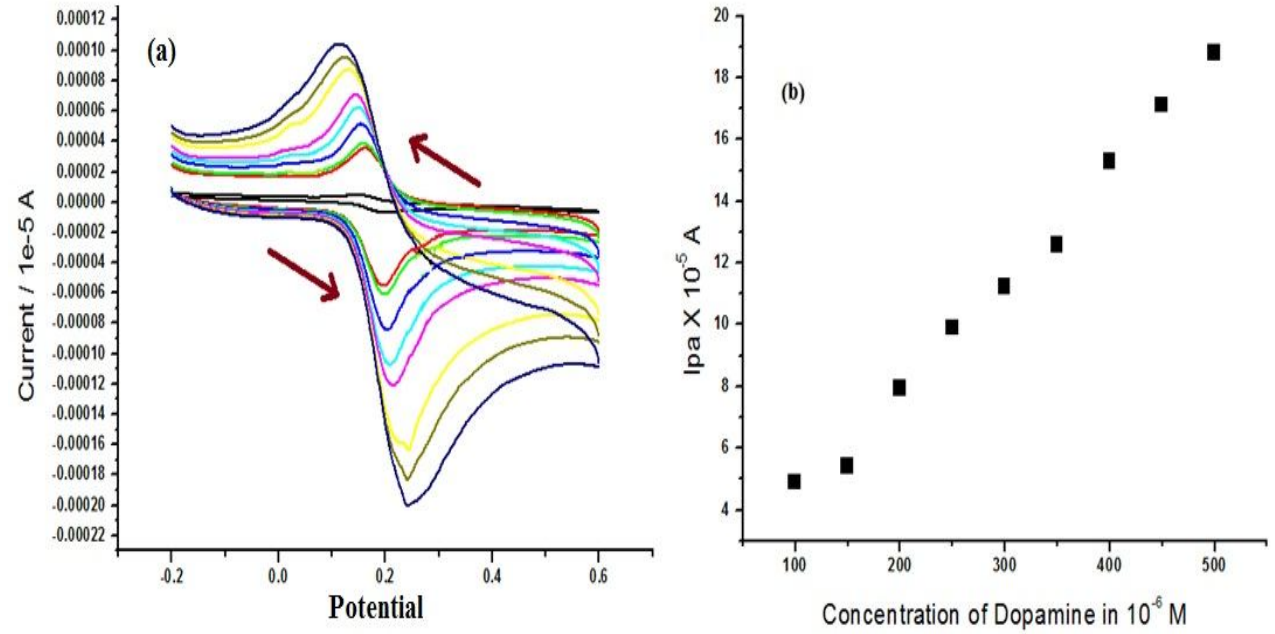

Fig. 15. (a) Cyclic voltammograms obtained for different concentrations of dopamine (50 µM to 500 µM) in PBS of pH 7 at scan rate 100 mV s^{-1}. (b) Graph of concentration of the dopamine *vs*. anodic peak current.

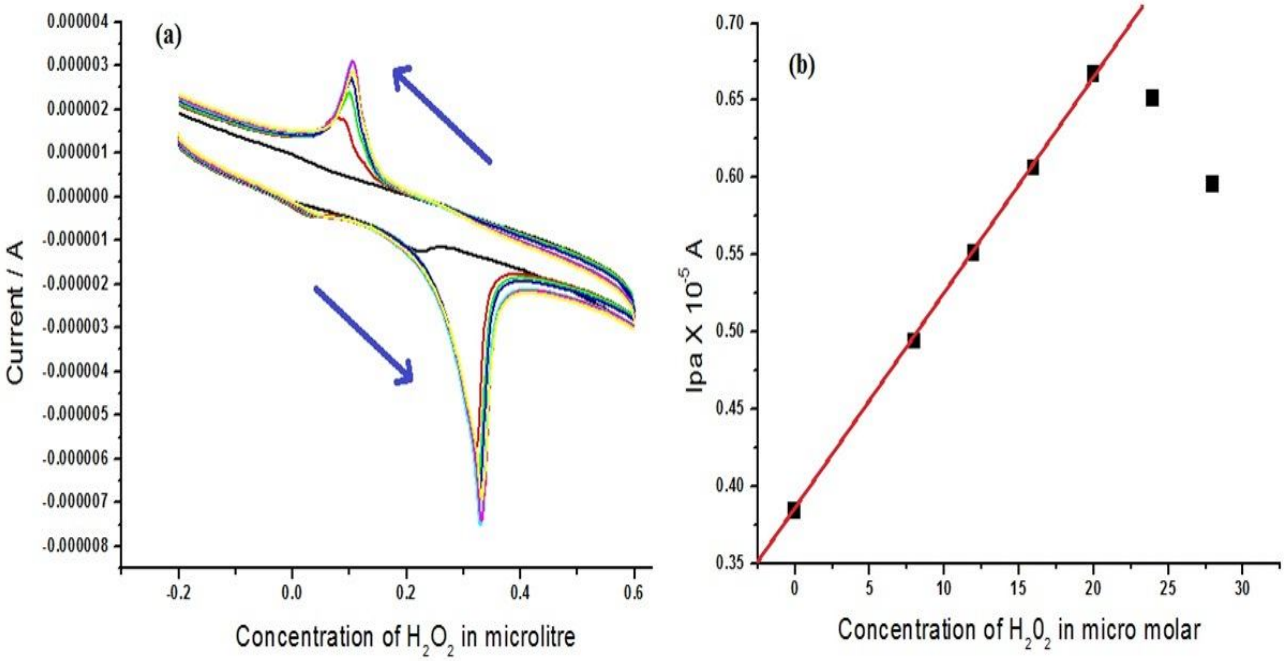

Fig. 16. (a) Cyclic voltammograms obtained for different concentrations of H_2O_2 (8 µM to 28 µM) in PBS of pH 7 at scan rate 100 mV s^{-1}. (b) Graph of concentration of H_2O_2 *vs*. anodic peak current.

the cyclic voltammograms of 20 μM hydrogen peroxide at various scan rates (0.1-0.8 V s^{-1}). The graph obtained was a straight line passing through the origin with a correlation coefficient of r^2 = 0.9973 for DA and that of H_2O_2 is r^2 = 0.9863. This confirms that the electron transfer reaction in the present work is diffusion-controlled [31].

Effect of concentration of dopamine and H_2O_2. According to the electrochemical response, the anodic peak current increases with increasing the concentration of DA and H_2O_2. Carbon paste with silicone oil, modified with 40 μl of silver nanoparticles was used to study the variation of analyte concentration.

Figure 15a depicts the voltammogram obtained using MCPE at different concentrations of dopamine (50 to 500 μM). Similarly, Fig. 16a represents the voltammogram obtained at different concentrations of H_2O_2 (8 to 28 μM). The graph of anodic peak current against the concentration of dopamine showed a linear relationship in the range 50-500 μM as shown in Fig. 15b. Similarly, the graph of anodic peak current against the concentration of H_2O_2 shows a linear relationship in the range 8-20 μM as shown in Fig. 16b. In case of H_2O_2, the relationship between the response current and the concentration starts to deviate rapidly from the straight line at the concentration higher than 20 μM. Thus, the silver nanoparticle modified carbon paste electrode can be used to determine the concentration of H_2O_2 in the range between 8 μM and 20 μM, whereas in the case of dopamine, as the concentration of dopamine increases the response current also increases linearly. Therefore, in the present work, we got maximum anodic peak current at 20 μM for H_2O_2 and 500 μM for dopamine, respectively.

CONCLUSIONS

Colloidal silver nanoparticles were synthesized successfully from the aqueous extract of leaves of acacia melanoxylon. The prepared silver nanoparticle modified CPE is more effective in investigating the electrochemical properties of bioactive DA and H_2O_2. The fabricated silver nanoparticle modified carbon paste electrode exhibits a diffusion-controlled process and enhanced electrochemical sensing property for the detection of dopamine and hydrogen peroxide at physiological pH. Therefore, the present method could be extended to various metals for the fabrication of modified electrodes with good electrocatalytic activities for the investigation of ascorbic acid, uric acid, and other bioactive molecules or neurotransmitters. The zeta potential of prepared silver nanoparticles is found to be -22.75 mV. Thermal analysis was carried out to study the stability of prepared silver nanoparticles. Thermogravimetric analysis shows 23.24% weight loss and DSC curve shows exothermic peak at 169 °C and Tg at 427 °C, respectively.

REFERENCES

[1] Sastry, M.; Ahmad, A.; Khan, M. I.; Kumar, R., Microbial nanoparticle Production, in Nanobiotechnology, Niemeyer CM and Mirkin CA, Eds., Wiley-VCH, Weinheim, Germany, 2004.

[2] Gardea-Torresdey, J. L.; Parsons, J. G.; Gomez, E.; Peralta-Videa, J.; Troiani, H. E.; Santiago, P., Formation and growth of Au nanoparticles inside live alfalfa plants. *Nano Lett.* **2002**, *2*, 397-401, DOI: 10.1021/nl015673+.

[3] Chandran, S. P.; Chaudhary, M.; Pasricha, R.; Ahmad, A.; Sastry, M., Synthesis of gold nanotriangles and silver nanoparticles using Aloe vera plant extract. *Biotechnol. Prog.* **2006**, *22*, 577-583, DOI: 10.1021/bp0501423.

[4] Huang, J.; Li, Q.; Sun, D.; Lu, Y.; Su, Y.; Yang, X., Biosynthesis of silver and gold nanoparticles by novel sundried Cinnamomum camphora leaf. *Nanotechnology.* **2007**, *18*, 105104-105115, DOI: 10.1088/0957-4484/18/10/105104.

[5] Mukherjee, P.; Roy, M.; Mandal, B.; Dey, G.; Mukherjee, P.; Ghatak, J.; Tyagi, A. K.; Kale, S. P., Green synthesis of highly stabilized nanocrystalline silver particles by a non-pathogenic and agriculturally important fungus T. asperellum. *Nanotechnology.* **2008**, *19*, 75103-75110, DOI: 10.1088/0957-4484/19/7/075103.

[6] Harekrishna, B.; Dipak, K. B.; Gobinda, P. S.; Priyanka, S.; Sankar, P. D.; Ajay, M., Green synthesis of silver nanoparticles using latex of Jatropha curcas. *Colloids and Surfaces A: Physicochem. Eng. Aspects.* **2009**, *339*, 134-139, DOI: 10.1016/

j.colsurfa.2009.02.008.

[7] Porter, T., Wood: Identification and Use, East Sussex, GB: Guild of Master Craftsman Publications Ltd. 2006, 37.

[8] Mohanpuria. P.; Rana, N. K.; Yadav, S. K., Biosynthesis of nanoparticles: Technological concepts and future applications. *J. Nanopart. Res.* **2008**, *10*, 507-517, DOI: 10.1007/s11051-007-9275-x.

[9] Guascito, M. R.; Filippo, E.; Malitesta, C.; Manno, D.; Serra, A.; Turco, A., A new amperometric nanostructured sensor for the analytical determination of hydrogen peroxide. *Biosens Bioelectron.* **2008**, *24*, 1057-1063, DOI: 10.1016/j.bios.2008.07.048.

[10] Sawa, A.; Snyder, S. H., Schizophrenia: diverse approaches to a complex disease. *Science.* **2002**, *296*, 692-695, DOI: 10.1126/science.1070532.

[11] Wightman, R. M.; May, L. J.; Michael, A. C., Detection of dopamine dynamics in the brain. *Anal Chem.* **1988**, *60*, 769A-779A, DOI: 10.1021/ ac00164a001.

[12] Krishnan, C. V., Garnett, M.; Chu, B., Oxidative stress and parkinson's disease: Electrochemical behavior of hydrogen peroxide in aqueous sodium chloride. *Int. J. Electrochem. Sci.* **2008**, *3*, 1348-1363.

[13] Yavich, L.; Tiihonen, J., *In vivo* voltammetry with removable carbon fibre electrodes in freely-moving mice: dopamine release during intracranial self-stimulation. *J. Neurosci. Methods.* **2000**, *104*, 55-63, DOI: 10.1016/s0165-0270(00)00321-6.

[14] Wang, J.; Martinez, T.; Yaniv, D. R.; McCornick, L., Characterization of the microdistribution of conductive and insulating regions of carbon paste electrodes with scanning tunneling microscopy. *J. Electroanal Chem.* **1990**, *286*, 265-272, DOI: 10.1016/0022-0728(90)85079-K.

[15] Shashanka, R.; Chaira, D.; Swamy, B. E. K., Electrocatalytic response of duplex and yittria dispersed duplex stainless steel modified carbon paste electrode in detecting folic acid using cyclic voltammetry. *Int. J. Electrochem. Sci.* **2015**, *10*, 5586-5598.

[16] Shashanka, R.; Chaira, D.; Swamy, B. E. K., Electrochemical investigation of duplex stainless steel at carbon paste electrode and its application to the detection of dopamine, ascorbic and uric acid. *Int. J. Scientific & Engin. Res.* **2015**, *6*, 1863-1871.

[17] Sathish, R.; Swamy, B. E. K.; Aruna, S.; Kumar, M.; Shashanka, R.; Jayadevappa, H., Preparation of NiO/ZnO hybrid nanoparticles for electrochemical sensing of dopamine and uric acid. *Chem. Sensors.* **2012**, *2*, 1-7.

[18] Shashanka, R.; Swamy, B. E. K.; Sathish, R.; Chaira, D., Synthesis of silver nanoparticles and their applications. *Anal. Bioanal. Electrochem.* **2013**, *5*, 455-466.

[19] Shashanka, R.; Chaira, D., Phase transformation and microstructure study of nano-structured austenitic and ferritic stainless steel powders prepared by planetary milling. *Powder Technol.* **2014**, *259*, 125–136, DOI: 10.1016/j.powtec.2014.03.061.

[20] Shashanka, R.; Chaira, D., Development of nanostructured duplex and ferritic stainless steel by pulverisette planetary milling followed by pressureless sintering. *Mater Charact.* **2015**, *99*, 220-229, DOI: 10.1016/j.matchar.2014.11.030.

[21] Gupta, S.; Shashanka, R.; Chaira, D., Synthesis of nano-structured duplex and ferritic stainless steel powders by planetary milling: An experimental and simulation study. *IOP Conf. Series: Materials Sci. Engin.* **2015**, *75*, 012033, DOI: 10.1088/1757-899X/75/1/012033.

[22] Nayak, A. K.; Shashanka, R.; Chaira, D., Effect of nanosize yittria and tungsten addition to duplex stainless steel during high energy planetary milling. *IOP Conf. Series: Materials Sci. Engin.* **2016**, *115*, 012008, DOI: 10.1088/1757-899X/115/1/012008.

[23] Shashanka, R., Effect of sintering temperature on the pitting corrosion of ball milled duplex stainless steel by using linear sweep voltammetry. *Anal. Bioanal. Electrochem.* **2018**, *10*, 349-361.

[24] Shashanka, R., Non-lubricated dry sliding wear behavior of spark plasma sintered nano-structured stainless steel. *J. Mater. Environ. Sci.* **2019**, *10*, 767-777.

[25] Shashanka, R.; Kamacı, Y.; Taş, R.; Ceylan, Y.; Bülbül, A. S.; Uzun, O.; Karaoglanli, A. C., Antimicrobial investigation of CuO and ZnO nanoparticles prepared by a rapid combustion method.

Phys. Chem. Res. **2019**, *7*, 799-812, DOI: 10.22036/pcr.2019.199338.1669.

[26] Shashanka, R.; Chaira, D., Optimization of milling parameters for the synthesis of nano-structured duplex and ferritic stainless steel powders by high energy planetary milling. *Powder Technol.* **2015**, *278*, 35-45, DOI: 10.1016/j.powtec.2014.03.061.

[27] Park, J. -Y.; Lee, Y. -J.; Jun, K. -W.; Baeg, J. -O.; Yim, D. J., Chemical synthesis and characterization of highly oil dispersed MgO nanoparticles. *J. Ind. Eng. Chem.* **2006**, *12*, 882-887.

[28] Narayanan, K. B.; Sakthivel, N., Coriander leaf mediated biosynthesis of gold nanoparticles. *Mater Lett.* **2008**, *62*, 4588-4590.

[29] Jain, N.; Bhargava, A.; Majumdar, S.; Tarafdar, J. C.; Panwar, J., Extracellular biosynthesis and characterization of silver nanoparticles using Aspergillus flavus NJP08: A mechanism perspective. *Nanoscale.* **2011**, *3*, 635-641.

[30] Shashanka, R., Synthesis of nano-structured stainless steel powder by mechanical alloying-an overview. *Int. J. Sci. Engin. Res.* **2017**, *8,* 588-594.

[31] Shashanka, R.; Chaira, D.; Swamy, B. E. K., Fabrication of yttria dispersed duplex stainless steel electrode to determine dopamine, ascorbic and uric acid electrochemically by using cyclic voltammetry. *Int. J. Sci. Engin. Res.* **2016**, *7*, 1275-1285.